Available online at www.sciencedirect.com

SciVerse ScienceDirect

Ceramics International 39 (2013) S637–S640

CERAMICS INTERNATIONAL

www.elsevier.com/locate/ceramint

# Electrochemical properties of $Ba(MnPO_4)_2 \cdot H_2O$ in alkaline aqueous electrolytes

Yusuke Kintsu[a], Shinya Suzuki[a], Masaru Miyayama[a,b,*]

[a]RCAST, The University of Tokyo, Tokyo 153-8904, Japan
[b]JST, CREST, Tokyo 102-0075, Japan

Available online 17 October 2012

**Abstract**

$Ba(MnPO_4)_2 \cdot H_2O$ and $Ba(MnPO_4)_2 \cdot H_2O$/carbon composites were synthesized by a hydrothermal process and their electrochemical properties were evaluated in 1 M KOH aqueous solution. $Ba(MnPO_4)_2 \cdot H_2O$ mixed with carbon particles (BMP/Cmix) showed a reversible capacity of 54 mAh $g^{-1}$ in a potential range of $-0.3 \sim +0.5$ V. Although it showed a large irreversible capacity when measured in $-1.0 \sim +0.6$ V, a structural change into $Mn_3O_4$ occurred. $Ba(MnPO_4)_2 \cdot H_2O$/ carbon composites (BMP/Ccom) showed a good cycling performance and kept larger capacities than BMP/Cmix at high current densities above 1000 mA $g^{-1}$.


*Keywords:* B. Nanocomposites; E. Batteries; E. Electrodes; Manganese phosphates

## 1. Introduction

Demands of large-capacity and high-power energy storage devices are increasing rapidly in applications for power tools and electric vehicles. Electrochemical capacitors (ECs) have recently been studied extensively because of their excellent storage properties, high safety and long cycle life [1]. Electrochemical capacitors store energy through faradic reduction/oxidation reactions of active materials at and near their surface, in addition to electric double layer capacitance [2,3].

Many kinds of transition-metal oxides have been researched for electrode materials of electrochemical capacitors [4]. Hydrous ruthenium dioxides ($RuO_2$) are known to show a high specific capacitance and cycling performance by protons adsorbing at an electrode surface and running into the bulk [4,5]. However, its commercial application is limited by the high-cost. Manganese dioxides ($MnO_2$) have been focused on as an alternative to $RuO_2$ because they are low-cost, nontoxic, abundant in raw materials and have a wide range of valence of Mn from +4 to +2 in alkaline media [6]. The $MnO_2$ electrodes exhibit comparably high, stable specific capacities in neutral aqueous electrolyte [7,8] and larger capacities are expected in alkaline solutions. However, when the reactions between $Mn^{4+}$ and $Mn^{2+}$ occur in alkaline solutions, a structural change occurs from $MnO_2$ into spinel-structured $Mn_3O_4$ and this gives degradation (lowering of capacity) of the $MnO_2$ electrodes [9,10].

In the present study, barium manganese phosphate $Ba(MnPO_4)_2 \cdot H_2O$ (expressed as BMP, hereafter) [11,12] was selected as an alternative to the electrode materials for electrochemical capacitors, because the phosphate groups in the material were expected to improve structural stability. There has been no report on the electrochemical properties in aqueous electrolytes except $LiMnPO_4$ [13]. Layered barium manganese phosphates [$Ba(MnPO_4)_2 \cdot H_2O$] mixed with carbon particles (expressed as BMP/Cmix, hereafter), and $Ba(MnPO_4)_2 \cdot H_2O$/ carbon composites (expressed as BMP/Ccom) were synthesized and their electrode properties were examined in 1 M KOH aqueous electrolytes.

## 2. Experimental section

### 2.1. Synthesis and characterization

$Ba(MnPO_4)_2 \cdot H_2O$ was synthesized under hydrothermal conditions [11]. An aqueous solution (20 mL) of $MnCl_2 \cdot$

*Corresponding author at: RCAST, The University of Tokyo, Tokyo 153-8904, Japan. Tel.: +81 3 5452 5037; fax: +81 3 5452 5083.
*E-mail address:* miyayama@rcast.u-tokyo.ac.jp (M. Miyayama).

0272-8842/$ - see front matter © 2013 Published by Elsevier Ltd and Techna Group S.r.l.
http://dx.doi.org/10.1016/j.ceramint.2012.10.152

$4H_2O$ (4.38 mmol), $H_3PO_4$ (8.40 mmol) and $Ba(OH)_2 \cdot 8H_2O$ (2.19 mmol) was prepared. The pH of the solution was adjusted to 11 by adding 40% methylamine. The mixture was heated at 170 °C for 72 h in a stainless steel autoclave under autogeneous pressure. The product was separated by filtration and washed with deionized water. $Ba(MnPO_4)_2 \cdot H_2O$/ carbon composites (BMP/Ccom) was synthesized from the solution of $MnCl_2 \cdot 4H_2O$, $H_3PO_4$, $Ba(OH)_2 \cdot 8H_2O$, methylamine, mixed with hydrophilic acetylene black, in the same hydrothermal condition. The hydrophilic acetylene black was prepared by stirring acetylene black in a mixed acid of 98% sulfuric acid and 60% nitric acid (3:1 vol%). The amount of hydrophilic acetylene black was adjusted to be 50 wt% of BMP/Ccom.

Thermal decompositions of the product were investigated by thermogravimetric analysis (TG–DTA). The TG–DTA experiments were carried out in air on a Rigaku Thermo Plus TG 8120 by increasing temperature at a rate of 10 $Kmin^{-1}$ from 50 °C to 800 °C with calcined $Al_2O_3$ powder as the standard reference.

The structures of the prepared products were studied by X-ray powder diffraction using a Bruker D8 Advance powder diffractometer with CuKα radiation ($\lambda$=0.1546 nm). The morphologies of samples were examined with scanning electron microscopy (SEM) using a Hitachi S–4500 after gold coating.

### 2.2. Electrochemical properties

The BMP/Cmix electrodes were prepared by mixing 45 wt% of BMP powder as active material with 45 wt% of acetylene black and 10 wt% of polytetrafluoroethylene (PTFE). The BMP/Ccom electrodes were prepared by mixing 90 wt% of BMP/Ccom with 10 wt% of PTFE. These mixtures were pressed onto a titanium mesh connected to a titanium wire.

Galvanostatic charge–discharge tests were performed at a current density of 100 mA $(g\text{-BMP})^{-1}$ with a Solartron 1470E CellTest system. Cyclic voltammetry (CV) tests were carried out at a scanning rate of 0.5 $mVs^{-1}$ using HZ–3000. A piece of platinum gauze and an Hg/HgO electrode were assembled as the counter and reference electrode, respectively. 1 M KOH aqueous solution was used as the electrolyte.

## 3. Results and discussion

The XRD patterns of BMP and BMP/Ccom are shown in Fig. 1(a) and (b), respectively. All detectable peaks were indexed as $Ba(MnPO_4)_2 \cdot H_2O$. In addition, a broad peak of carbon was observed at around 2θ=25° for BMP/Ccom.

The TG curve of $Ba(MnPO_4)_2 \cdot H_2O$ showed a weight loss between 300 °C and 400 °C which was related to the release of crystallization waters, while a weight loss attributed to a carbon decomposition was also observed over 500 °C in BMP/Ccom. The weight ratio of BMP and carbon in BMP/Ccom was calculated to 47: 53.

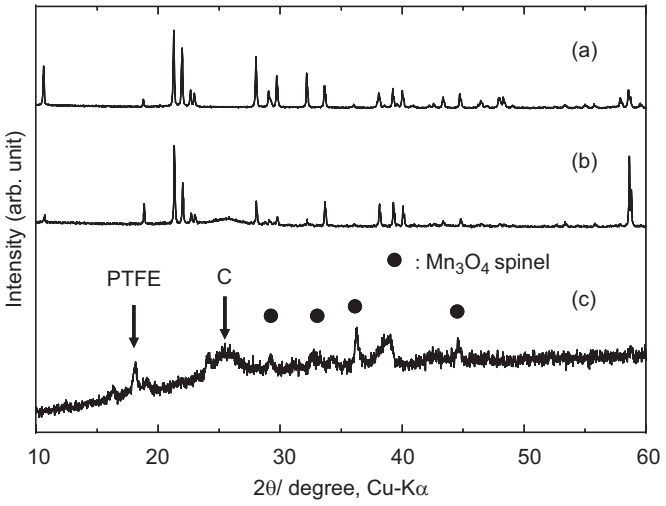


Fig. 1. The XRD patterns of (a) BMP, (b) BMP/Ccom, (c) BMP/Cmix after the 40th cycle (in −1.0∼+0.6 V).

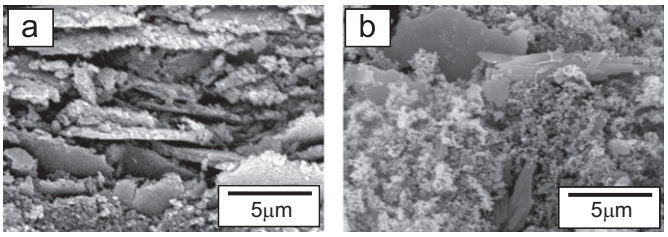


Fig. 2. SEM images of (a) BMP/Cmix and (b) BMP/Ccom.

SEM images of BMP/Cmix and BMP/Ccom are shown in Fig. 2. Most of BMP particles were in plate-like shape, and the lateral size was 5–10 μm. The aggregations of BMP particles were observed in the BMP/Cmix, while BMP particles seem to be mixed homogeneously with carbon particles in the BMP/Ccom.

Fig. 3 shows a cyclic voltammogram of BMP/Cmix measured in a potential range of −1.0∼+0.6 V (vs. Hg/HgO). Two peaks were observed on oxidation and reduction processes, suggesting Mn redox reactions between $Mn^{4+}$ and $Mn^{2+}$.

Cycling performances of discharge capacities obtained from galvanostatic charge–discharge tests are shown in Fig. 4. The capacity of BMP/Cmix measured in the potential range of −1.0∼+0.6 V, Fig. 4(a), showed a gradual increase of capacity to 129 mAh $(g\text{-BMP})^{-1}$ at the 16th cycle, followed by a gradual decrease. This capacity value corresponds to 1.09 times larger than that assuming 1-electron reaction of Mn ions, suggesting occurrence of partial 2-electron reaction of Mn ions. Since the XRD pattern of BMP/Cmix after the 40th cycle had peaks of $Mn_3O_4$ spinel as shown in Fig. 1(c), the capacity peak is attributed to an irreversible change to the $Mn_3O_4$ spinel having $Mn^{2+}$ and $Mn^{3+}$. However, the capacity degradation is not so rapid as observed in $MnO_2$ [10], and then the BMP was found to be more stable than $MnO_2$ in alkaline aqueous solutions.

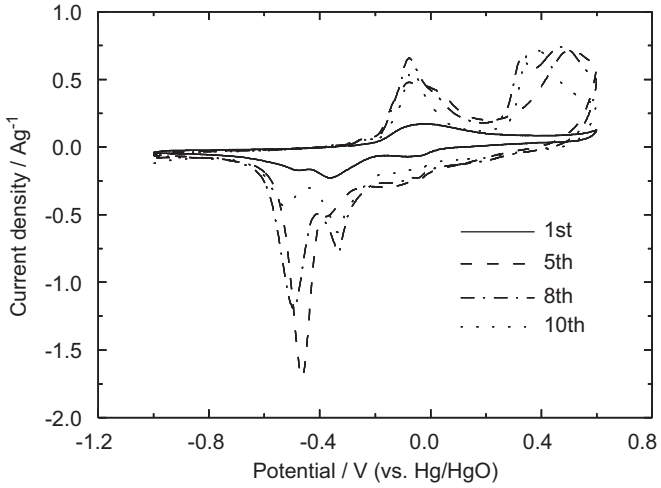


Fig. 3. Cyclic voltammogram of BMP/Cmix measured in −1.0∼+0.6 V.

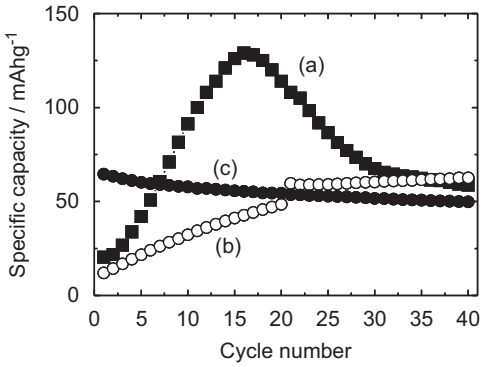


Fig. 4. Cycling performances of (a) BMP/Cmix (−1.0∼+0.6 V), (b) BMP/Cmix (−0.3∼+0.5 V), and (c) BMP/Ccom (−0.3∼+0.5 V).

From comparison with cyclic voltammogram of $MnO_2$ [9,10], the current peak at −0.45 V during reduction process in Fig. 3 was suggested to originate from the formation of $Mn_3O_4$. Therefore, galvanostatic charge–discharge measurements were conducted for BMP/Cmix in a potential range of −0.3∼+0.5 V to inhibit the $Mn_3O_4$ formation. Charge–discharge curves at the 40th cycle and cycling performance of the BMP/Cmix are shown in Fig. 5(a) and Fig. 4(b), respectively. Charge–discharge curves showed continuous slopes without an evident plateau. On the cycling performance, although the capacity increased with cycles in the initial stage, a stable capacity of 54 mAh $(g\text{-}BMP)^{-1}$ was obtained after the 20th cycle. This capacity value is in the same level with that of $MnO_2$ in a neutral electrolyte [7,10]. Furthermore, the structure of BMP was maintained without transformation into $Mn_3O_4$ after the 80th cycle.

Charge–discharge curves at the 40th cycle and cycling performance are shown in Fig. 5(b) and Fig. 4(c), respectively. The composite electrode showed a discharge capacity of 65 mAh $(g\text{-}BMP)^{-1}$ from the 1st cycle, and maintained the capacity of 50 mAh $(g\text{-}BMP)^{-1}$ after the 80th cycle.

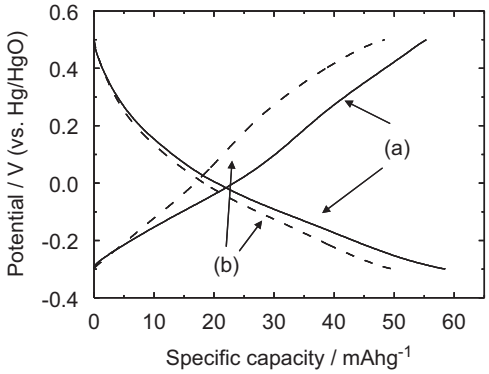


Fig. 5. Charge–discharge curves of (a) BMP/Cmix and (b) BMP/Ccom at the 40th cycle (100 $mAg^{-1}$, −0.3∼0.5 V).

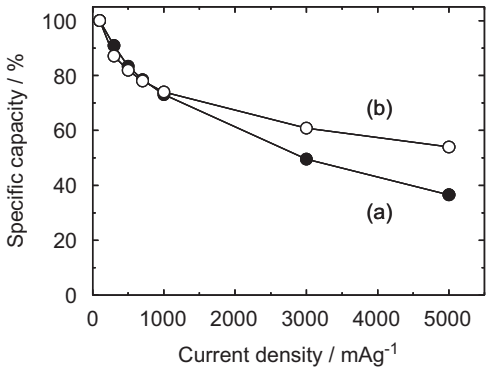


Fig. 6. Rate performances of (a) BMP/Cmix and (b) BMP/Ccom, both in −0.3∼+0.5 V.

Fig. 6 shows the ratio of capacities measured at various current densities to that measured at 100 mA $(g\text{-}BMP)^{-1}$. The BMP/Ccom kept a larger capacity than BMP/Cmix at high current densities above 1000 mA $(g\text{-}BMP)^{-1}$. Electronic conductivity of BMP (without carbon) estimated from DC I–V relations of BMP pressed compact in air was as low as the order of $10^{-8}$ $Scm^{-1}$. Accordingly, formation of highly conductive electrodes is necessary for rapid charge/discharge properties. The stable cyclability shown in Fig. 4(c) and good rate performance in Fig. 6 of BMP/Ccom are considered to originate from smooth electron transfer between BMP and carbon particles due to homogeneous composite structure with conductive carbons.

## 4. Conclusions

Electrodes of simple mixtures and homogeneous composites of $Ba(MnPO_4)_2 \cdot H_2O$ and carbon were synthesized and their electrochemical properties were evaluated in 1 M KOH aqueous solution. The BMP/Cmix showed a discharge capacity of 129 mAh $(g\text{-}BMP)^{-1}$ in a potential range of −1.0 – +0.6 V, suggesting partial 2-electron reaction of Mn ions, but a structural change into $Mn_3O_4$ and capacity degradation were observed after cycling. By adjusting the potential range to −0.3 – +0.5 V, the BMP/Cmix

exhibited reversible capacities of 54 mAh (g-BMP)$^{-1}$ without structural change into $Mn_3O_4$. The BMP/Ccom showed stable discharge capacities of 50 mAh (g-BMP)$^{-1}$ and kept a larger capacity than BMP/Cmix at large current densities above 1000 mA (g-BMP)$^{-1}$.

## References


[1] B.E. Conway, Transition from supercapacitor to battery behavior in electrochemical energy storage, Journal of the Electrochemical Society 138 (1991) 1539–1548.

[2] J.P. Zheng, J. Huang, T.R. Jow, The limitations of energy density for electrochemical capacitors, Journal of the Electrochemical Society 144 (1997) 2026–2031.

[3] S. Sarangapani, B.V. Tilak, C.-P. Chen, Materials for electrochemical capacitors, Journal of the Electrochemical Society 143 (1996) 3791–3799.

[4] J.P. Zheng, T.R. Jow, A new charge storage mechanism for electrochemical capacitors, Journal of the Electrochemical Society 142 (1995) L6–L8.

[5] K. Naoi, S. Ishimoto, N. Ogihara, Y. Nakagawa, S. Hatta, Encapsulation of nanodot ruthenium oxide into KB for electrochemical capacitors, Journal of the Electrochemical Society 156 (2009) A52–A59.

[6] Y.S. Jun, S.T. Martin, Microscopic observations of reductive manganite dissolution under oxic conditions, Environmental Science and Technology 37 (2003) 2363–2370.

[7] Y.U. Jeong, A. Manthiram, Nanocrystalline manganese oxides for electrochemical capacitors with neutral electrolytes, Journal of the Electrochemical Society 149 (2002) A1419–A1422.

[8] S.-C. Pang, M.A. Anderson, T.W. Chapman, Novel electrode materials for thin-film ultracapacitors: comparison of electrochemical properties of sol–gel-derived and electrodeposited manganese dioxide, Journal of the Electrochemical Society 147 (2000) 444–450.

[9] J. McBreen, The electrochemistry of β-$MnO_2$ and γ-$MnO_2$ in alkaline electrolyte, Electrochimica Acta 20 (1975) 221–225.

[10] H. Jang, S. Suzuki, M. Miyayama, Electrode properties of nanosheet-derived $MnO_2$ for electrochemical capacitors, ECS Transactions 33 (2011) 145–154.

[11] J. Escobal, J.L. Mesa, J.L. Pizarro, L. Lezama, R. Olazcuaga, T. Rojo, Hydrothermal synthesis, structural, spectroscopic and magnetic studies of a lamellar phosphate: $Ba(MnPO_4)_2 \cdot H_2O$, Journal of Materials Chemistry 9 (1999) 2691–2695.

[12] X. Bu, P. Feng, G.D. Stucky, A lamellar hydrated barium cobalt phosphate with a two-dimensional array of Co–O–Co network: $Ba(CoPO_4)_2 \cdot H_2O$, Journal of Solid State Chemistry 131 (1997) 387–393.

[13] M. Minakshi, P. Singh, S. Thurgate, K. Prince, Electrochemical behavior of olivine-type $LiMnPO_4$ in aqueous solutions, Journal of Electrochemical and Solid-State Letters 9 (2006) A471–A474.